International Journal of Nanomedicine

Dovepress

open access to scientific and medical research

Open Access Full Text Article

ORIGINAL RESEARCH

Sericin/Nano-Hydroxyapatite Hydrogels Based on Graphene Oxide for Effective Bone Regeneration via Immunomodulation and Osteoinduction

Mei Fu[1], Jun Li[2], Mingchong Liu[1], Chensong Yang[1], Qidong Wang[1], Hongrui Wang[3], Bingdi Chen[2], Qingge Fu[3], Guixin Sun[1]

[1]Department of Traumatic Surgery, Shanghai East Hospital, School of Medicine, Tongji University, Shanghai, People's Republic of China; [2]Institute for Regenerative Medicine, Shanghai East Hospital, The Institute for Biomedical Engineering & Nano Science, School of Medicine, Tongji University, Shanghai, People's Republic of China; [3]Department of Orthopedic Trauma, Changhai Hospital, Naval Medical University (Second Military Medical University), Shanghai, People's Republic of China

Correspondence: Guixin Sun; Qingge Fu, Email sunguixin@tongji.edu.cn; fqg7821@163.com

Background: Immune responses and osteogenesis differentiation induced by implants are crucial for bone tissue regeneration. Consideration of only one of those properties is not sufficient. To investigate the synergistic actions, we designed alginate/graphene oxide/sericin/nanohydroxyapatite (Alg/GO/Ser/nHAP) nanocomposite hydrogels with both osteoimmunomodulatory and osteoinductive activities. This study aimed to explore the effect of hydrogel with osteoimmunomodulatory properties on promoting osteogenesis of bone marrow stem cells (BMSCs).

Methods: Alg/GO/Ser/nHAP nanocomposite hydrogel was fabricated and was characterized by SEM, FTIR, XRD, stress-strain, rheology, swelling and degradation. After the impact of sericin on M2 macrophage polarization was identified, the BMSCs viability and adhesion were evaluated by CCK8 assay, live/dead staining, cytoskeleton staining. The cell osteogenic differentiation was observed by ALP/ARS staining, immunofluorescence staining, RT-PCR, and Western blotting, respectively. Rat cranial defect model was used to assess osteoimmunomodulatory effects of scaffolds in vivo by micro-computed tomographic, histological, and immunohistochemical analyses after 8 weeks of healing.

Results: In vitro experiments revealed that the hydrogel presented desirable mechanical strength, stability, porosity, and biocompatibility. Significantly, sericin and nHAP appeared to exert synergistic effects on bone regeneration. Sericin was observed to inhibit the immune response by inducing macrophage M2-type polarization to create a positive osteoimmune microenvironment, contributing to improving osseointegration at the bone-implant interface to promote osteogenesis. However, the osteogenic differentiation in rat BMSCs was further enhanced by combining nHAP and sericin in the nanocomposite hydrogel. Eventually, the hydrogel was implanted into the rat cranial defect model, assisting in the reduction of local inflammation and efficient bone regeneration.

Conclusion: The nanocomposite hydrogel stimulated bone formation by the synergistic effects of immunomodulation of macrophage polarization by sericin and direct osteogenic induction by nHAP, demonstrating that such a scaffold that modulates the osteoimmune microenvironment to promote osteogenesis is a promising approach for the development of bone tissue engineering implants in the future.

Keywords: hydrogel, nano-hydroxyapatite, sericin, osteoimmunomodulation, osteoinduction, bone regeneration

Introduction

Throughout the world, the healing and regeneration of severe bone defects caused by heavy limb damage, bone tumors, and infectious illnesses continue to be a serious therapeutic challenge, bringing serious disturbances to the patient.[1,2] Autogenous bone implants were once regarded as the gold standard due to their histocompatibility and osteoinductive and nonimmunogenic activities; However, their use is currently restricted due to the shortage of autograft supplies, the threat of infection, and other intraoperative complications.[3,4] To solve this issue, an alternative for the healing of bone

Received: 7 December 2022
Accepted: 5 April 2023
Published: 6 April 2023

Graphical Abstract

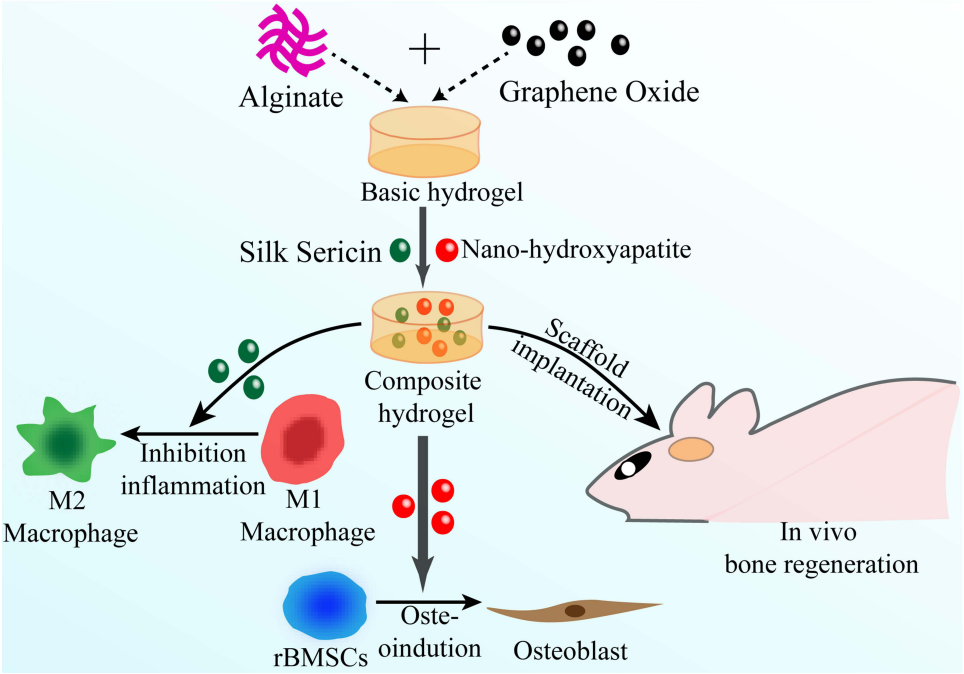

repair has emerged in the form of bone tissue engineering in the last few years.[5] Nevertheless, the previous design of biomaterials primarily concentrated on accelerating the direct osteogenesis of planting cells without considering biomaterial-induced immune reactions.[6] It has been reported that the host immune system frequently recognizes implanted biomaterials as unwanted objects and sets off a chain of immunological reactions that can result in fibrotic encapsulation, implant instability, or implantation failure.[7] Hence, not only the direct osteogenesis effect but also the immunomodulatory activity of biomaterials should be considered to maximize the efficacy of bone regeneration when developing a suitable bone implant.[8]

Macrophages are among the most essential effector cells in the immunological microenvironment formed by implanted biomaterials and play a significant role in determining the performance of bone substitute implantation.[2] It has been proposed that as important immune responder cells, macrophages can initiate and regulate inflammatory activity during an immunological response.[9] These cells can be stimulated to present corresponding phenotypes in dynamic response to different environmental stimuli due to their high plasticity.[10] As shown in earlier research, macrophages transforming into the M1 phenotype secrete a massive amount of proinflammatory cytokines, such as interleukin 1 (IL-1), interleukin 6 (IL-6), tumor necrosis factor-alpha (TNF-α) and inducible nitric oxide synthase (iNOS), which cause persistent inflammation and fibrous encapsulation surrounding the implanted materials, eventually contributing to osseointegration failure.[11,12] In contrast, cells that switch to the M2 phenotype are capable of releasing anti-inflammatory cytokines, such as arginine-1 (Arg-1), interleukin 4 (IL-4), and interleukin 10 (IL-10), to inhibit the inflammatory response[11,13] and other bioactive molecules, such as bone morphogenetic protein 2 (BMP-2), bone morphogenetic protein 4 (BMP-4), vascular endothelial growth factor (VEGF), and transforming growth factor-β (TGF-β) to accelerate angiogenesis and osteogenesis, which are all valuable for the establishment of a bone regeneration environment.[14] Therefore, the favorable immunomodulatory microenvironment induced by M2 macrophage polarization is essential for bone repair. Different measures have been taken to regulate the local immunological microenvironment surrounding bone implants, such as changing the mechanical and chemical characteristics of biomaterials, modifying

surface physical features, and introducing bioactive molecules or cytokines.[2,9,15] However, few investigations on the regulatory effects of natural polymers on macrophages have been conducted.

Silk sericin (SS), a low-cost glycoprotein manufactured as a byproduct of the silk industry, is one of the two principal proteins that make up silkworm cocoons together with silk fibroin.[16] As a natural polymer, sericin has been confirmed to show a weak immune response due to its high concentration of serine, which accounts for 33% of total hydrophilic amino acids and is the most abundant amino acid.[17,18] According to studies, modified serine biomaterials can resist foreign body reactions.[19] However, the mechanical strength and osteoinductive capacity of the protein are inadequate, limiting its use as a high-performance biopolymer, which can be improved by incorporating nanomaterials with appropriate properties.[20] Moreover, aside from regulating the immunological microenvironment, osteoinductive capacity seems to be another appealing property of optimal artificial bone implantation.[3] Nano-hydroxyapatite (nHAP), as the most abundant inorganic component of bone, has been widely used in tissue regeneration due to its outstanding bone regeneration capabilities, including extraordinary biocompatibility, direct osteoinduction, and excellent mechanical properties.[21,22] Therefore, the combination of nHAP and natural polymers may allow for increasing the mechanical strength of the implant to achieve a better outcome of bone regeneration.

To create an ideal biological milieu for cell attachment, growth, and differentiation, a desirable implant should possess great biocompatibility and suitable physical properties.[23] For example, graphene oxide (GO), which is classified as a type of highly dispersible nanomaterial with a thin layer of carbon atoms with sp2 hybridization, a broad area of the specific surface, and excellent strength,[24] has been thoroughly explored for its possibilities as a potential material for the formation of new bone due to its optimal characteristics of osteogenesis induction and mechanical behavior. In addition, it can enhance the ability of BMSCs to differentiate into osteoblasts by interacting with proteins via stacking, hydrogen bonding, electrostatic interactions, etc.[25] On the other hand, alginates (Alg), as one of the most frequently utilized supporting components, are commonly employed in bone tissue engineering owing to a variety of characteristics, including gelling ability, nontoxicity, availability, and affordability. In addition, superior biocompatibility makes it possible for alginate to provide an ideal environment for the adhesion and bone regeneration of BMCSs.[23]

Despite the individual usage of either sericin or nHAP in biomaterials that have been explored by previous studies, their synergistic therapeutic effects on bone regeneration are still unknown. Therefore, we developed the nanocomposite hydrogel Alg/GO/Ser/nHAP using the cross-linking system of calcium disodium EDTA and D-(+)-gluconic acid δ-lactone (EDTA-2Ca/GDL). Experiments were carried out to evaluate the effect of the composite hydrogel on osteogenic differentiation. The findings showed that the fabricated nanocompound hydrogel could promote bone regeneration in vitro and in vivo through the synergistic effect of immunoactive sericin and osteoinductive nHAP on macrophage polarization and osteogenesis (Figure S1). In conclusion, our results indicated that the Alg/GO/Ser/nHAP hydrogel was an excellent and safe implant to accelerate new bone formation via direct osteoinductive and osteoimmunomodulatory dual functions. Furthermore, the hydrogel may offer an easy and efficient alternative for the development of biomaterials that can establish a supportive osteoimmunomodulatory microenvironment in vivo for the recovery of bone defects, with potential applications in orthopedic surgery in the future.

Material and Methods

Materials

Information on access to all materials and reagents used in this study is presented in the Supplementary Information (SI) (Sections S1.1).

Preparation of Hydrogels

For the fabrication of different hydrogels, several stock solutions were prepared. A known volume of GO powder or nHAP was dispersed into distilled water completely by ultrasonic oscillation and then stored at 4°C for use later. Followingly, by adding an appropriate amount of Alg and EDTA-2Ca to distilled water and then mixing it with the stock solution of GO, thus the basic hydrogel premixture (Alg/GO-pre) was developed, with the final concentrations of EDTA-2Ca in the mixture being 5mg/mL. After initially mixing, the premixture was subjected to 30 minutes of ultrasonic oscillation accompanied by 4 hours of continuous magnetic stirring, and then an appropriate amount of GDL powder was added to the premixture for another 30 minutes. Ultimately, the basic hydrogel (Alg/GO) was finished by loading the

mixture into 12-well plates overnight to crosslink. In this study, the properties of three distinct composite hydrogel scaffolds were explored: Alg/GO/Ser, Alg/GO/nHAP, and Alg/GO/Ser/nHAP, abbreviated as Ser, nHAP, and S+H, respectively. Therefore, the solutions of sericin, nHAP, and sericin+nHAP were individually added to the basic hydrogel premixture (Alg/GO-pre). Subsequently, the same protocol of the preparation of the basic hydrogel (Alg/GO) was repeated for the preparation of composite hydrogels, with the final concentrations of Alg, GO, nHAP, and sericin in hydrogels being 2wt%, 0.1mg/mL, 1wt%, 2wt% correspondingly. All three types of hydrogel scaffolds (Alg/GO/Ser, Alg/GO/nHAP, Alg/GO/Ser/nHAP) were sterilized with the application of ethylene oxide before use.

Characterization of Hydrogels

To further explore the relevant properties of hydrogels fabricated in this study, the experiment of transmission electron microscope (TEM), scanning electron microscopy (SEM), Fourier transform infrared (FTIR), X-ray diffraction (XRD), stress/strain test and rheological were carried out separately, and the details were in Section S1.2–S1.5 in the SI, respectively.

Porosity Analysis

Liquid displacement was used to measure the porosity of different hydrogels, and the details were in Section S1.6 in the SI.

Swelling Study

By soaking the scaffold in 1×PBS at specific time intervals, the swelling ratio of different hydrogels was measured, and the details were in Section S1.7 in the SI.

Degradation in vitro

To measure the stability of hydrogel scaffold structure in vitro, the degradation performance of samples was analyzed in this work, and the details were in Section S1.8 in the SI.

Isolation and Culture of BMSCs and Macrophages

The details of isolation and culture for BMSCs and rat peritoneal macrophages were in Section S1.9 in the SI. BMSCs of passages 3 to 5 were employed.

In vitro Biocompatibility of Hydrogels

The viability and morphology of cells were evaluated by the cell counting kit-8 (CCK-8) cell proliferation assay, live/dead staining, TRITC Phalloidin cytoskeleton staining, and the details were in Section S1.10 in the SI.

Macrophage M2-Type Differentiation Induced by Hydrogels

The macrophage (2×10^5 cells per well) was inoculated in the bottom chamber of a 24-well transwell plate and was treated with 200 ng/mL lipopolysaccharide (LPS, Sigma) for 24 hours to induce the M1 phenotype. After induction, cells were further treated with different hydrogel scaffolds placed in the upper chamber of the 24-well transwell plate. In the control group, only DMEM was used. After 24 hours of culture with different gels, cells were collected to assess polarization status using Western blot (WB), immunofluorescence (IF) staining, as well as RT-qPCR. The primer sequences of the related genes were listed in Table S1.

Osteogenesis Differentiation and Mineralization of BMSCs in vitro

To assess the osteogenic differentiation capacity of BMSCs, the experiment of alkaline phosphatase (ALP) staining, Alizarin Red S (ARS) staining, WB, IF and RT-qPCR were performed respectively, and the details were in Section S1.11–S1.14 in the SI. The primer sequences of the related genes were listed in Table S1.

Preparation of macrophage conditioned medium (MCM) composed of different hydrogels.

In an attempt to find out whether the osteogenesis differentiation capacity of BMSCs could be influenced by macrophage polarization, the corresponding macrophage-conditioned mediums (MCM) were prepared. In brief,

macrophages were incubated in 6-well plates (1×10^5 cells per well) overnight, and then stimulated with 200ng/mL LPS for 24 hours, and co-cultured with various hydrogel scaffolds for additional 24 hours. Following that, the supernatant from each sample was harvested, centrifuged at 1000 rpm for 5 minutes, and filtered with a 0.22μm filter to eliminate any remaining cells before being refrigerated at −80°C for subsequent BMSCs co-cultivation. For each experiment, MCM was prepared by mixing the supernatant with fresh DMEM media at a 1:1 v/v ratio.

BMSCs osteogenesis differentiation induced by macrophage conditioned medium (MCM).

BMSCs (1×10^6 cells per mL) were grown in DMEM for 12 h, and then the medium was changed with the MCM containing osteogenesis elements (50μg/mL ascorbic acid, 1×10^{-8}M dexamethasone, and 10mM β-glycerol phosphate) for further cultivation. To evaluate osteogenesis differentiation, IF, ALP activity, ALP staining, RT-qPCR analysis, and WB were performed after 7 days as previously described. The degree of calcification of cells was assessed after 21 days of cultivation by staining for ARS.

In vivo Experiments

For the purpose of evaluating the impact of different hydrogel scaffolds implanted in vivo on the repair of bone defects, a rat calvarial defect model was prepared, and the details were in Section S1.15 in the SI. The animal experiments performed in this study were permitted and carried out according to the rules of the Animal Ethics Committee of Tongji University (Ethics Resolution Number: TGAA07221403). The surgeries were performed following the National Institutes of Health (NIH) Guide for the Care and Use of Laboratory Animals. After 8 weeks of implantation, cranial samples were gathered and fixed in 4% PFA for 24 hours at room temperature to assess the impact of bone defect healing following the implantation of various scaffolds. The experiment of micro-CT, staining of H&E, Masson, and immunohistochemical (IHC) were conducted respectively, and the details were in Section S1.16–S1.18 in the SI.

Statistical Analysis

All experiments involved three independent (n=3) trials. Data were displayed as mean ± SD. The statistical analysis was conducted by the one-way analysis of variance (ANOVA) followed by Tukey's multiple comparison tests to assess the differences between groups. The value of $P<0.05$ was considered statistically significant.

Results

Fabrication and Characterization of the Hydrogel

In this study, the basic hydrogel (Alg/GO) scaffold consisted of alginate, GO, EDTA-2Ca and GDL. After adding different components, including sericin, nHAP, and sericin+nHAP, to the basic hydrogel, Alg/GO/Ser, Alg/GO/nHAP, and Alg/GO/Ser/nHAP hydrogels were separately prepared successfully and defined as groups Ser, nHAP, and S+H, respectively. The pure Alg gel was transparent, and the overall appearance of the Alg/GO gel was clear brown after adding GO. When further mixed with sericin, the Alg/GO/Ser gel took on a muddy brown appearance. Moreover, after adding nHAP, the appearance of the compound gel of both Alg/GO/nHAP and Alg/GO/Ser/nHAP was grey (Figure 1A). The morphology of pure GO and pure nHAP were observed by TEM, as shown in Figure S2 and Figure S3. The TEM image of GO plates showed a sheet-like morphology with a certain degree of transparency (Figure S2). Several GO layers or graphene layers formed a thick stacking nanostructure which presented the dark areas. At the same time, the nHAP particles were shown to have a short stick-like appearance (Figure S3). SEM analysis was used to observe the porous structure and surface morphology of the freeze-dried hydrogel scaffold composed of various components. All of the nanocomposite hydrogels exhibited a large number of open pores that were highly interconnected, and the pore size and porosity did not significantly alter after the addition of GO, although the inner wall roughness increased (Figure 1B). When sericin and nHAP particles were incorporated into the nanocomposite hydrogel, the porosities of Alg/GO/nHAP and Alg/GO/Ser/nHAP scaffolds were approximately 66.68% and 61.98%, respectively (Table S2).

The structural components of various hydrogels were investigated using FTIR spectroscopy (Figure 1C and D). The FTIR spectrum of the Alg/GO hydrogel showed absorbance bands at 1612 and 1418 cm^{-1}. The characteristic absorption peaks of sericin were at 1656, 1535, and 1239 cm^{-1}. After cross-linking with Alg/GO gel, the FTIR absorption spectrum of sericin in Alg/GO/Ser and Alg/GO/Ser/nHAP gels were marginally altered from 1656 to 1611 cm^{-1}, accompanied by

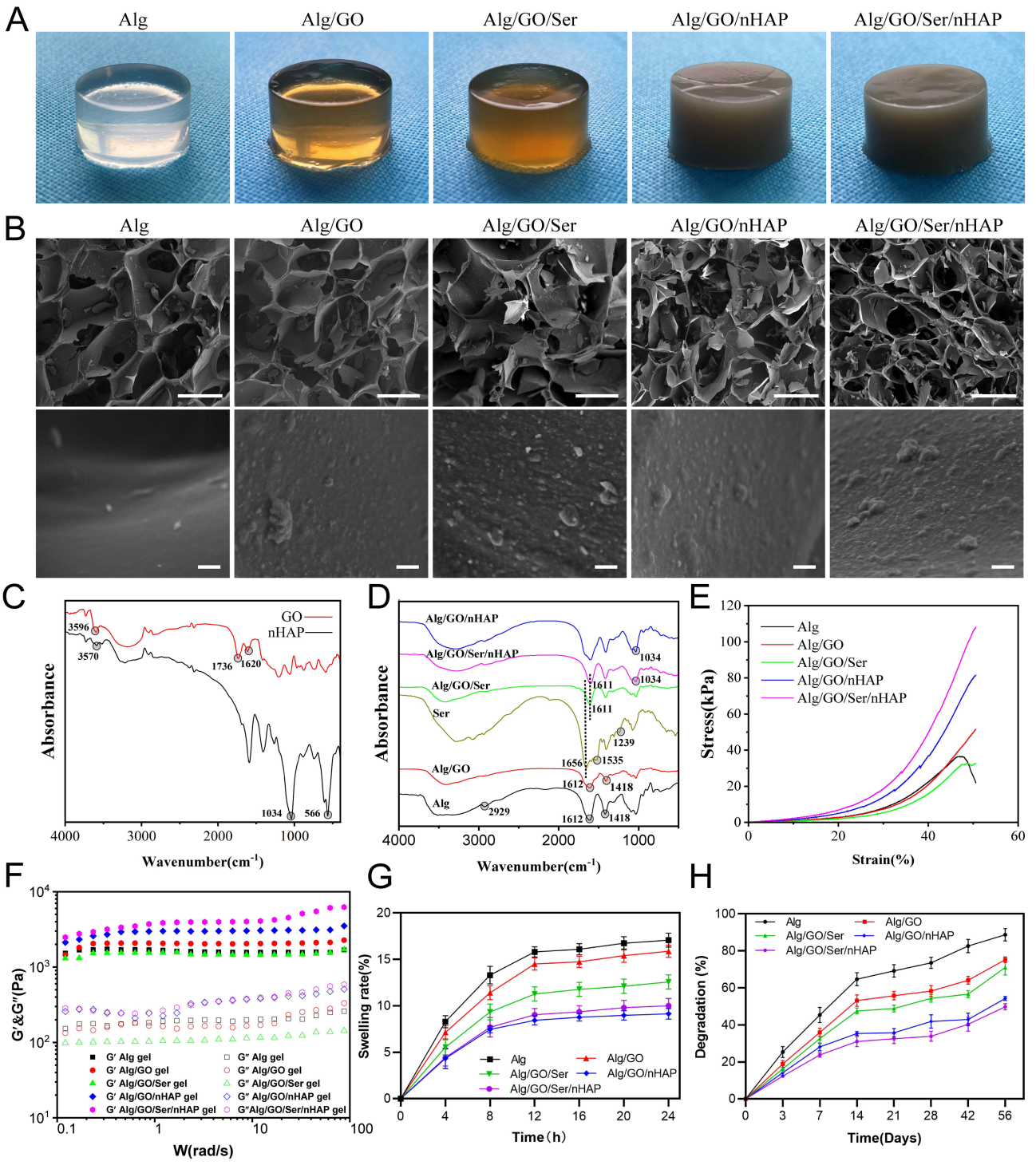

Figure 1 Characterization of different nanocomposite hydrogels. (**A**) The overall appearance of various hydrogels. (**B**) SEM images of different hydrogels. Scale bar=300μm (upper panel) and 10μm (lower panel). (**C**) FTIR spectra of GO, nHAP. (**D**) FTIR spectra of Alg, Alg/GO, Ser, Alg/GO/Ser, Alg/GO/Ser/nHAP, Alg/GO/nHAP. (**E**) Stress–strain curves of various hydrogels. (**F**) The storage modulus (G') and loss modulus (G'') values of the fabricated hydrogels. (**G**) The swelling rate of different hydrogels. (**H**) Degradation profiles of different hydrogels.

a decrease in the number of random coil absorption peaks (e g, 1535 and 1239 cm^{-1}). Additionally, the characteristic absorbance bands at 1034 cm^{-1} were shown in the FTIR spectra of the nanocomposite gel containing nHAP. Furthermore, an X-ray diffractometer was applied to analyze the impact of corresponding fillers on the alginate structural alterations, and the results were shown in Figure S4. The diffraction pattern of alginate displayed a shoulder peak at 13.6°

and a characteristic broad peak at 21.9°, suggesting a general amorphous structure. Meanwhile, these differently constituted hydrogels had diffraction peaks similar to those of the alginate, hence the incorporation of additional filler seems to have no effect on the crystalline peak of alginate, implying that Ca^{2+} crosslinking did not significantly influence crystallinity.

The strain–stress curves of various hydrogels are shown in Figure 1E. The compression modulus of the corresponding hydrogels was enhanced after the addition of nHAP, and the compression stress–strain graph revealed that the maximum strength of Alg/GO/Ser/nHAP was 109 kPa at 51.1% strain and that the compression modulus was 23.5 kPa. Based on the frequency- dependent oscillatory shear model, we performed rheological experiments to verify the formation of hydrogels. The storage modulus (G') and loss modulus (G") of the designed hydrogels are presented in Figure 1F. The hydrogels all exhibited a storage modulus greater than 1 kPa, indicating moderate mechanical properties and potential use as bone regeneration scaffolds. This result of rheological experiments demonstrated that the storage moduli of hydrogels were decreased when mixed with sericin but increased when nHAP was added. Additionally, we found that G' was highest in the Alg/GO/Ser/nHAP gel and lowest in the Alg/GO/Ser gel.

The swelling efficiency of different scaffolds was evaluated to examine the corresponding hydrophilicity. As illustrated in Figure 1G, the fabricated scaffolds exhibited different swelling rates. After 12 hours of immersion, all scaffolds displayed fast swelling potential and attained equilibrium, and then the swelling efficiency of all scaffolds slowly increased over time. The pure polymer scaffolds showed a higher swelling rate than the Alg/GO/Ser/nHAP nanocomposite scaffolds (9.1% to 17.2%). As shown in Figure 1H, the Alg gel was quickly degraded by lysozymes within the first 14 days, with a maximum degradation rate of approximately 65%. Nevertheless, after the addition of GO and nHAP, the degradation of the scaffold gradually weakened, since they experienced a slow degradation process with a degradation rate of approximately 30% within two weeks. After 8 weeks, the degradation of the pure Alg gel reached over 90%, whereas the degradation of the Alg/GO/Ser/nHAP scaffold reached approximately 45%.

Influences of Hydrogel on Cell Proliferation, Toxicity, and Adhesion

After 1, 3, and 7 days of incubation, the proliferation of BMSCs was assessed by CCK-8 assay. Figure 2A shows that the proliferation performance of BMSCs treated with various hydrogels was almost poor on the first day. As time passed, the viability of cells increased, and the proliferation rates of all groups increased with no significant differences between the different hydrogels. Using live/dead staining, we evaluated the toxicity of the scaffolds on BMSCs after 3 days of incubation with different hydrogels. Almost no dead cells were found in any of the groups, which suggested that all scaffolds had no cytotoxic influences on cells (Figure 2B). In addition, the result of cytoskeletal F-actin staining showed that after 1 day of culture, no remarkable differences in the adhesion or spreading of cells were found between different groups. In all groups, the morphology of BMSCs was mostly spherical with no or few filopodia. After 4 days of culture, cells treated with different hydrogels had a similar stretch pattern, and the number and spread area of cells were greater than those on the first day (Figure 2C), which indicated that the cells were connected, covered the scaffolds in polygonal forms and had a considerable expression of filamentous actin.

Macrophage Phenotype Regulated by Hydrogels

We investigated the effect of sericin on macrophage polarization to explore whether hydrogels containing sericin could immunomodulate the regeneration of new bone. In this work, rat peritoneal macrophages were isolated and identified successfully according to the methods of previous research (Figure S5). After being precultured with LPS for M1 polarization for approximately 24 hours, macrophages were incubated with different hydrogels for another 24 hours. IF staining, gene expression, and WB analysis were separately performed to examine the efficacy of each hydrogel scaffold in regulating inflammation. Proinflammatory cytokines and proteins, such as TNF-α and iNOS, have been identified as M1 phenotype indicators, whereas anti-inflammatory cytokines and proteins, including IL-10 and Arg-1, have been considered M2 phenotype markers.[26] As shown in IF staining, a lower proportion of iNOS positive cells and a higher percentage of Arg-1 positive cells were present in the Ser and S+H groups in comparison to the control and nHAP groups ($p<0.05$) (Figure 3A–C). WB analysis was further performed to indicate that hydrogels containing sericin (eg, the Ser and S+H groups) had decreased protein expression of iNOS and increased expression of Arg-1 compared to the nHAP and control groups ($p<0.05$) (Figure 3D–E). RT–qPCR analyses yielded similar results. Our findings demonstrated that the markers of the M1 phenotype, iNOS and TNF-α, were more highly expressed in the

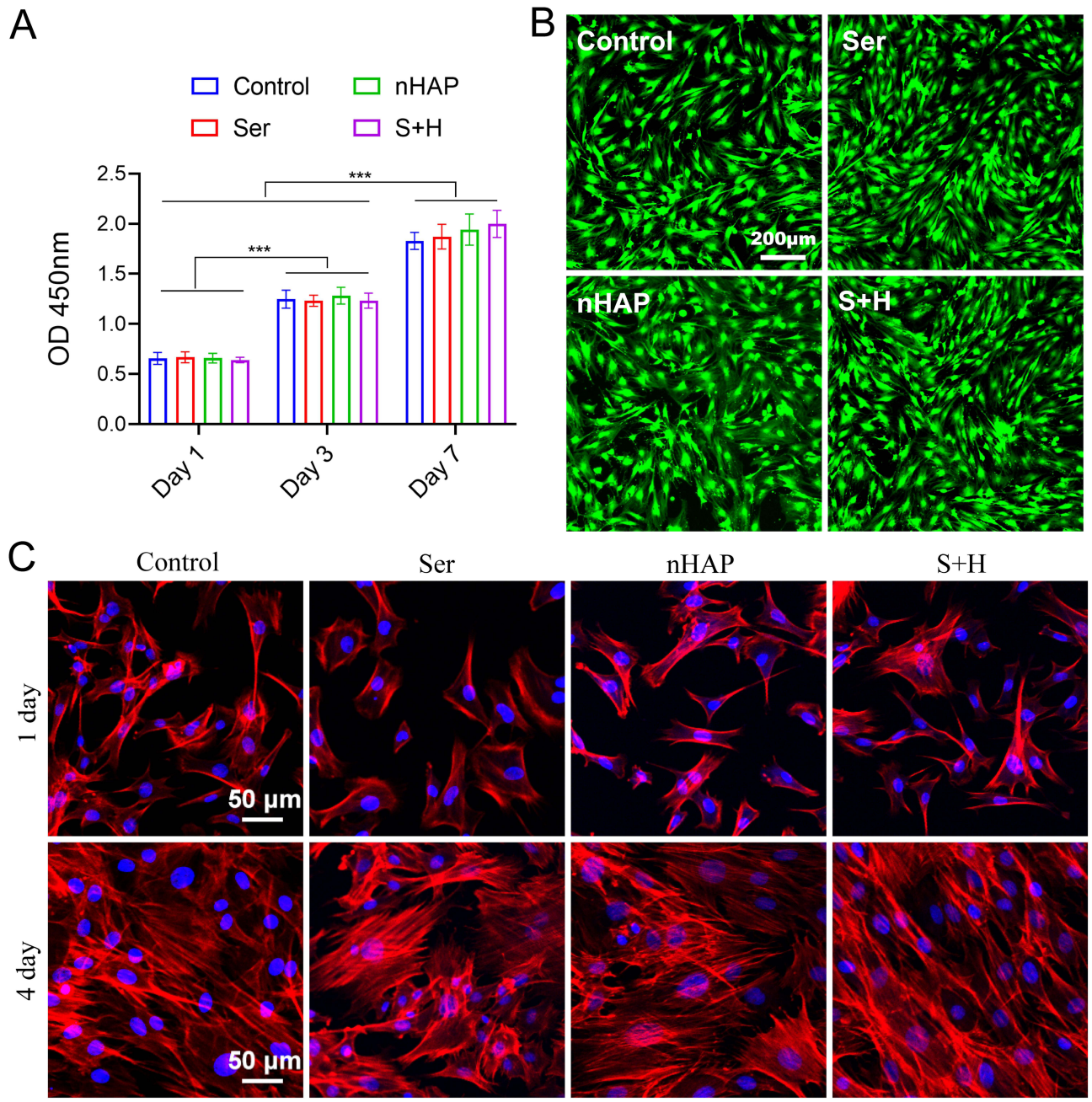

Figure 2 Biocompatibility properties of hydrogels. (**A**) The proliferation of BMSCs cultivated on various hydrogels for 1, 3, and 7 days. (**B**) The viability of BMSCs cultured with various hydrogels for 3 days was assessed by the live/dead staining. (**C**) The attachment of BMSCs seeded on the corresponding hydrogel after 1 and 4 days was exhibited in immunofluorescence images. Nuclei, blue; Cytoskeleton red. (***$p < 0.001$).

control and nHAP groups than in the Ser group and S+H group ($p<0.05$) (Figure 3F). At the same time, the markers of the M2 phenotype, IL-10 and Arg-1, were more highly expressed in the Ser and S+H groups than in the nHAP and control groups ($p<0.05$) (Figure 3F). Notably, throughout all experiments on the regulation of macrophage inflammation, no statistically significant differences were illustrated between the Ser and S+H or control and nHAP groups ($p<0.05$) (Figure 3A–F).

Direct Osteogenic Differentiation of BMSCs Induced by the Hydrogel

To assess the direct impact of the nanocomposite hydrogel on the regulation of osteogenesis, BMSCs were incubated with DMEM or hydrogel from different groups, and the osteogenic differentiation of cells was assessed by staining and

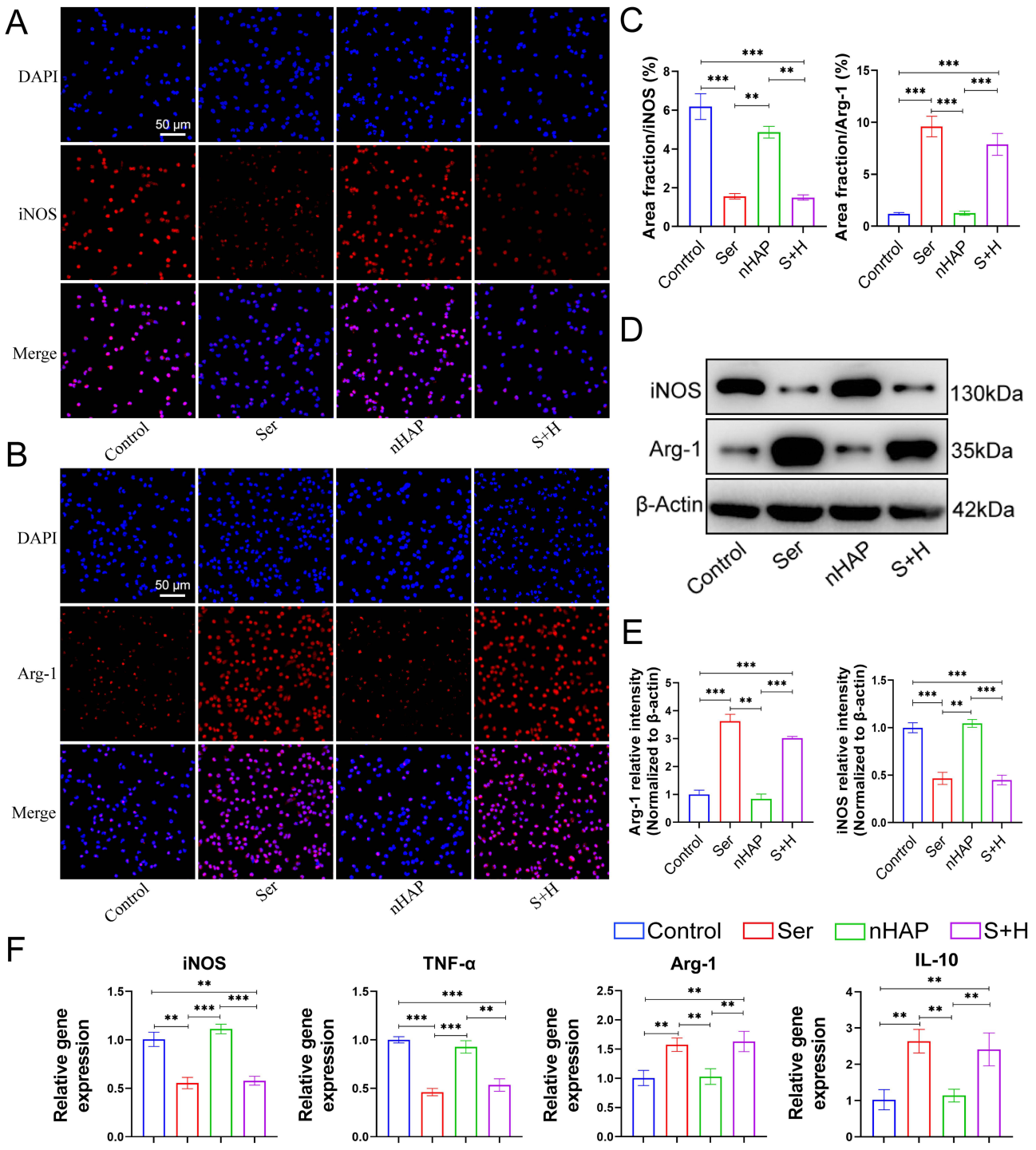

Figure 3 Effects of various hydrogels on regulating macrophage polarization. The macrophage was pre-cultured with LPS for 24 hours to induce M1 polarization and then incubated with the corresponding hydrogels for another 24 h. (**A**) iNOS and (**B**) Arg-1 IF staining of macrophages. Nuclei, blue; iNOS and Arg-1, red. (**C**) Quantitative analysis of IF for iNOS (left) and Arg-1 (right). (**D**) WB of the expression of Arg-1 and iNOS proteins. (**E**) Quantitative analysis of WB for Arg-1 (left) and iNOS (right). (**F**) The expressions of pro-inflammatory genes iNOS, TNF-α, and anti-inflammatory genes Arg-1, IL-10 were analyzed by RT-qPCR. (**p < 0.01, ***p < 0.001).

quantitative analysis of ALP and ARS. The results indicated that the S+H group showed the highest ALP activity and contained the largest number of mineralization nodules (Figure 4A–C). Similarly, the S+H group had dramatic upregulated expression of proteins associated with osteogenesis, including OPN and RunX2 (Figure 4D–H), and osteogenesis-associated genes, including RunX2, OPN, OCN, and COLI (Figure 4I) in comparison to the other three

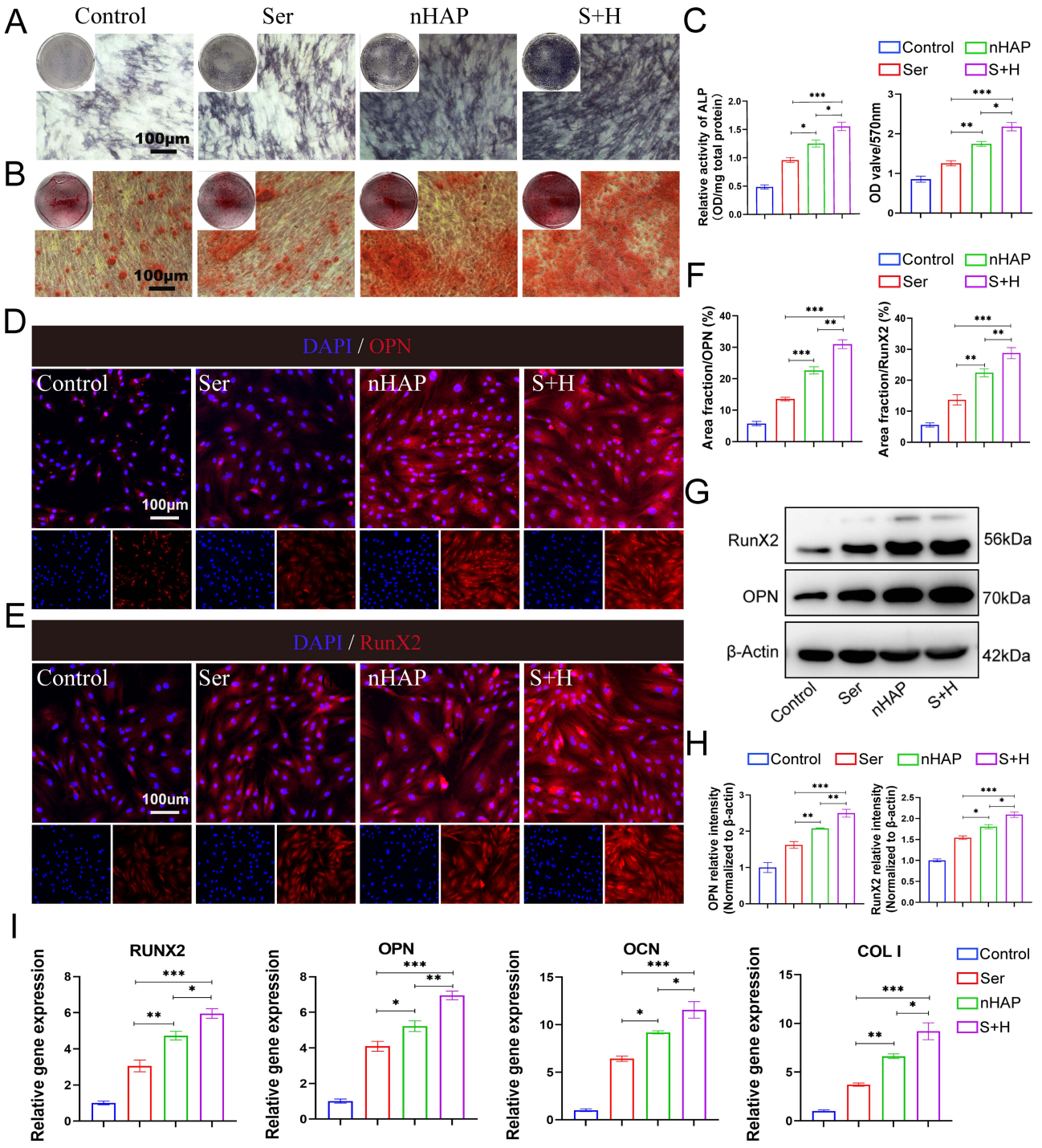

Figure 4 Osteogenesis of BMSCs induced by various hydrogels. (**A**) ALP staining after BMSCs treated with different hydrogels for 7 days. (**B**) ARS staining after BMSCs treated with different hydrogels for 21 days. (**C**) Normalized ALP activity (left) and semi-quantitative analysis of ARS staining (right). The IF for (**D**) OPN and (**E**) RunX2 of BMSCs after being treated with different hydrogels for 7 days. Nuclei, blue; OPN and RunX2, red. (**F**) Quantitative analysis of IF for OPN (left) and RunX2 (right). (**G**) WB of the expression of RunX2 and OPN protein for BMSCs cultured with scaffolds for 7 days. (**H**) Quantitative analysis of WB for OPN (left) and RunX2 (right). (**I**) RT-qPCR results of the gene expression related to osteogenesis (RunX2, OPN, OCN, and COLI) of BMSCs treated with different hydrogels for 7 days. (*p<0.05, **p<0.01, ***p <0.001).

groups (p<0.05). Herein, our findings indicated that the S+H hydrogel could lead to better osteogenesis induction via the synergistic modulatory effects of sericin and nHAP. Interestingly, the nHAP group consistently performed better than the Ser group in terms of the activity of ALP and the generation of mineralization nodules, as well as the expression of osteogenesis-related genes and proteins (p<0.05) (Figure 4A–I).

The Effect of M2-Polarized Macrophages on the Differentiation of BMSCs

By coculturing BMSCs with macrophage-conditioned medium (MCM) prepared with various nanohydrogels, the indirect influence of M2 macrophages on the osteogenic differentiation of BMSCs in vitro was investigated (Figure 5A). As indicated by the ALP and ARS data, BMSCs treated with the MCM of the Ser group were found to perform better in

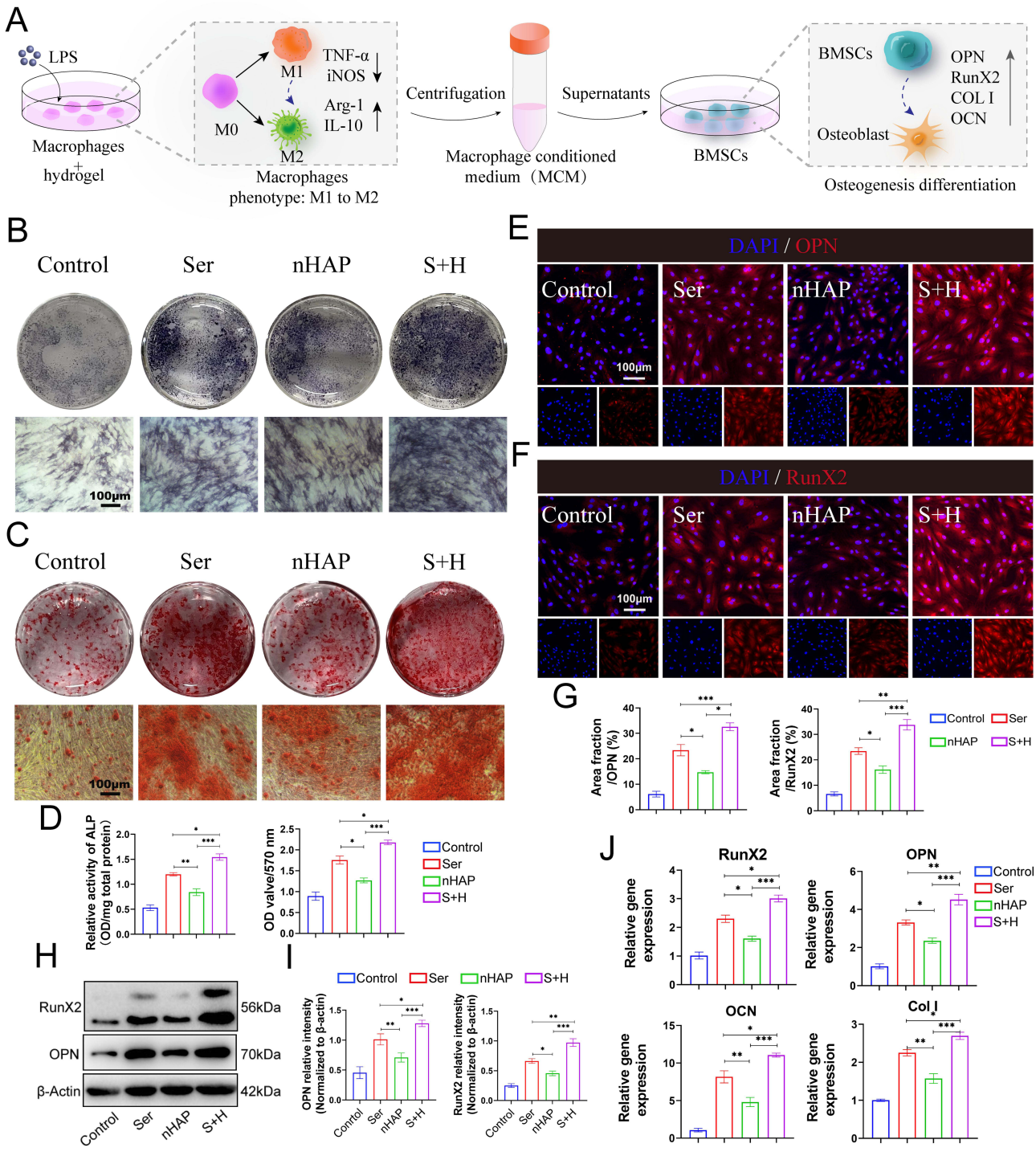

Figure 5 The influence of macrophage polarization on osteogenesis in BMSCs. (**A**) The illustration of experiment design. (**B**) ALP staining of BMSCs after induced using MCM for 7 days. (**C**) ARS staining of BMSCs after induced using MCM for 21 days. (**D**) Quantitative analysis of ALP activity (left) and ARS staining (right). The IF staining of (**E**) OPN and (**F**) RunX2 for BMSCs after induced using MCM for 7 days. Nuclei, blue; RunX2 and OPN, red. (**G**) Quantitative analysis of IF for OPN (left) and RunX2 (right). (**H**) WB detected Runx2 and OPN proteins in BMSCs after induced using MCM for 7 days. (**I**) Quantitative analysis of WB for OPN (left) and RunX2 (right). (**J**) RT-qPCR results of the gene expression related to osteogenesis (RunX2, OPN, OCN, and COLI) of BMSCs treated with different MCM for 7 days. (*p<0.05, **<p<0.01, ***p<0.001).

https://doi.org/10.2147/IJN.S399487 DovePress

regards to enhancing the activity of ALP and increasing the formation of mineralized nodules in comparison to the MCM of the nHAP group ($p<0.05$) (Figure 5B–D). Analogously, osteogenesis-related proteins, including OPN and RunX2 (Figure 5E–I), and osteogenesis-associated genes, including RunX2, OCN, OPN, and COLI (Figure 5J), were both higher in the MCM of the Ser groups than in the MCM of the nHAP group ($p<0.05$). In addition, the ALP and ARS data showed that the MCM prepared by the S+H group exhibited the highest degree of ALP expression and greatly enhanced the development of mineralized nodules in BMSCs compared with the other three groups ($p<0.05$) (Figure 5B–D). Analogously, BMSCs cocultured with the MCM of the S+H group presented the highest expression of osteogenesis-related proteins, including OPN and RunX2 (Figure 5E–I), as well as the highest expression of osteogenesis-related genes, including Runx2, OCN, OPN, and COLI, in comparison to the other three groups ($p<0.05$) (Figure 5J). Therefore, when cultured with macrophages, the ability of osteogenic induction of the Ser group was stronger than that of the nHAP group, while the ability of the S+H group was the strongest among all groups.

Bone Regeneration Potential in vivo and Histological Analysis

To assess the influences of the corresponding hydrogels on bone restoration in vivo, Alg/GO/Ser (Ser group), Alg/GO/nHAP (nHAP group), and Alg/GO/Ser/nHAP (S+H group) were separately implanted into the rat cranial defect model, and lacking hydrogels defined as the control group. After implantation for eight weeks, the rat cranial defect model was obtained and reconstructed utilizing micro-CT to provide photographs and perform the quantitative analysis of fresh bone generation. The degree of bone regeneration was in the sequence of S+H > Ser > nHAP > Control, as presented by micro-CT and histological observations (Figures 6A–D and 7A). The micro-CT photograph revealed that the bone defect area was mostly repaired after the S+H group scaffold was implanted. Furthermore, the Ser group had a higher degree of bone defect healing than the nHAP group. However, a large hollow defect remained in the control group, suggesting that the rat cranial defect model was effectively established (Figure 6A). The assessment of micro-CT showed that the S+H group exhibited the maximum bone volume per total volume (BV/TV), followed by the Ser, nHAP, and control groups ($p<0.05$) (Figure 6B).

Then, histological investigations, including H&E, Masson, and IHC staining, were performed to confirm the generation and maturity of fresh bone. H&E and Masson's staining revealed a great deal of fresh bone formation around the hydrogel in the S+H group, while moderate and little new bone tissue was present in the Ser and nHAP groups, respectively, and nearly no new bone tissue was found around the hydrogel of the control group (Figure 6C and D). This result demonstrated that the S+H group exhibited the strongest ability to stimulate bone defect healing in vivo, which was well supported by the micro-CT results. At the same time, both the control and nHAP group showed a thick continuous fibrous layer, whereas the Ser and S+H groups exhibited a thinner fibrous layer, which suggested that the in vivo implantation of the Ser and S+H group hydrogels resulted in a lower inflammatory response than that of the control or nHAP group, illustrating that the anti-inflammatory effects of sericin protein could help improve the process of osseointegration at the bone-implant interface (Figure 6C and D).

Furthermore, the outcomes of IHC staining of COLI revealed obvious positive staining of fresh bone in the S+H group, followed by the Ser, nHAP, and control group (Figure 7A). This result showed that the S+H scaffold stimulated more collagen matrix deposition compared to the other groups. In addition, the impact of immune regulation on osteogenesis was further evaluated by IHC staining of inflammation-related markers. At 8 weeks, IHC staining of the defect area suggested that more Arg-1 and less iNOS were present in the Ser and S+H groups than that in the nHAP and control groups (Figure 7B and C). Hence, the findings indicated that hydrogels containing sericin (eg, the Ser and S+H groups) could induce an anti-inflammatory environment between the implantation and the emerging bone tissue.

Discussion

Although bone tissue regeneration based on bone tissue engineering therapy has exhibited promising results in recent years, however, implantation failure frequently occurs due to the subsequent fibrous foreign body reaction.[27] Therefore, it is crucial to design implant materials that can modulate the macrophage immune response. Previous studies have reported that sericin can inhibit inflammatory response by inducing macrophage phenotype transformation.[28] While nHAP can directly induce osteogenic differentiation of BMSCs.[22] However, the synergistic effects of sericin and nHAP on bone

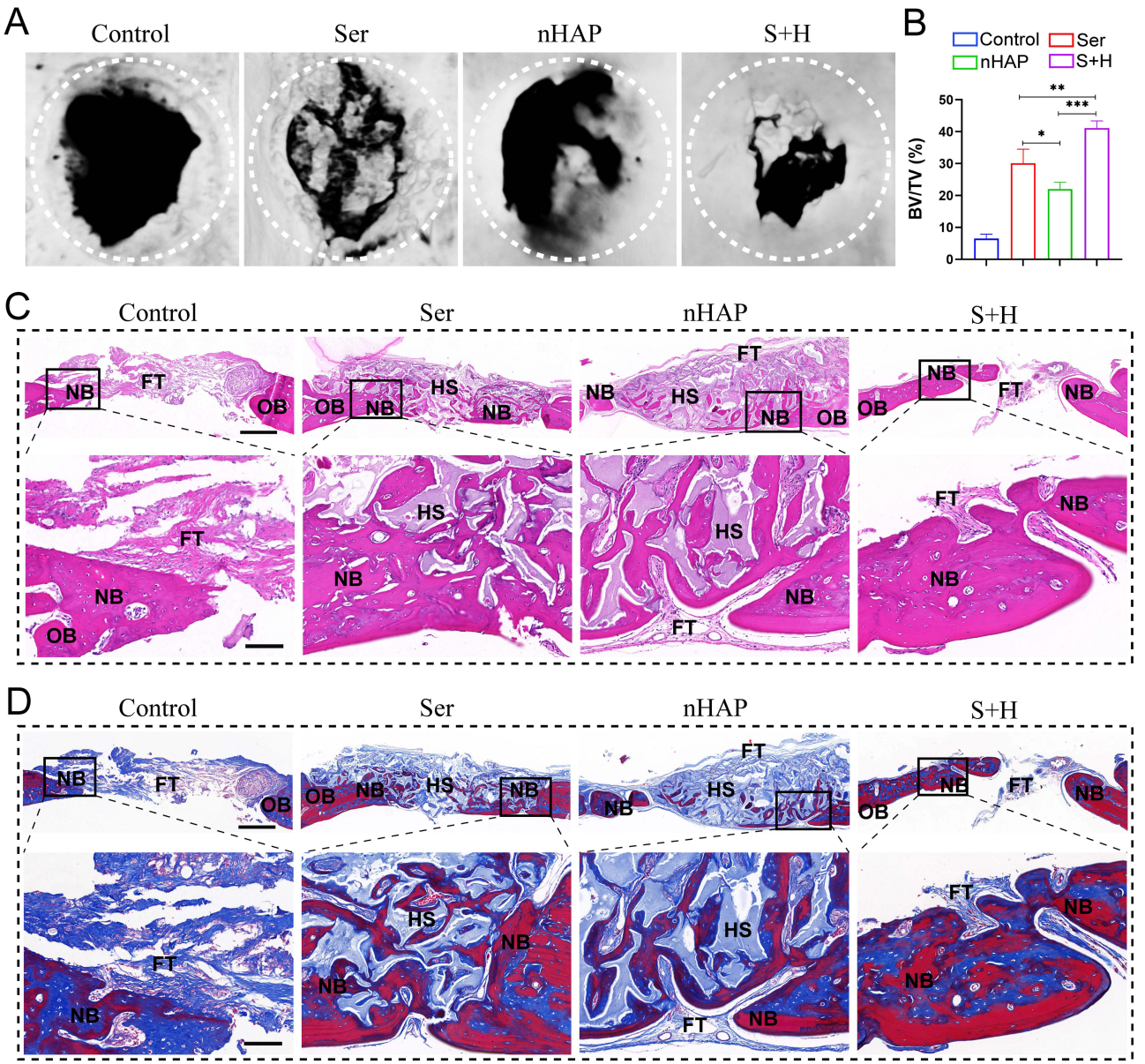

Figure 6 New bone regeneration property of different hydrogels in vivo. (**A**) After eight weeks of implantation, micro-CT pictures of cranial defects transplanted with various hydrogels or left unfilled were shown. (**B**) Quantitative analysis of BV/TV after implantation for 8 weeks. (**C**) Representative pictures of H&E staining after implantation for 8 weeks. (Scale bar: up=500μm, down=100μm). (**D**) Representative pictures of Masson staining after implantation for 8 weeks. (Scale bar: up=500μm, down=100μm). (OB, NB, FT, and HS symbolize original bone, new bone, fibrous tissue, and hydrogel scaffold, respectively). (*p<0.05, **p<0.01, ***p <0.001).

regeneration remain unknown. Therefore, we developed the nanocomposite hydrogel Alg/GO/Ser/nHAP based on a calcium ion cross-linking system and carried out a series of characterization experiments. In addition, we further evaluated in vivo and in vitro whether the nanocomposite scaffold could promote bone regeneration by regulating the anti-inflammatory phenotypic transformation of macrophages.

Due to the acidic environment generated by GDL, the calcium ions in EDTA-2Ca were slowly released, which could make the premixture into the basic gel (Alg/GO). It is well known that the gelation of alginate is commonly caused by the crosslinks of ionic cross-linkers (such as the divalent cation calcium), which crosslink the polymer chains through the "egg-box" model.[29,30] The fabrication of the nanocomposite hydrogels in this study was realized by molecular entanglement to form physical crosslinks. The image of SEM showed that the nanocomposite hydrogels not only had a porous structure, and their internal roughness also increased after the addition of GO (Figure 1B), which contributed to a favorable microenvironment for cell adhesion.[31] In addition, the porosities of Alg/GO/nHAP and Alg/GO/Ser/nHAP

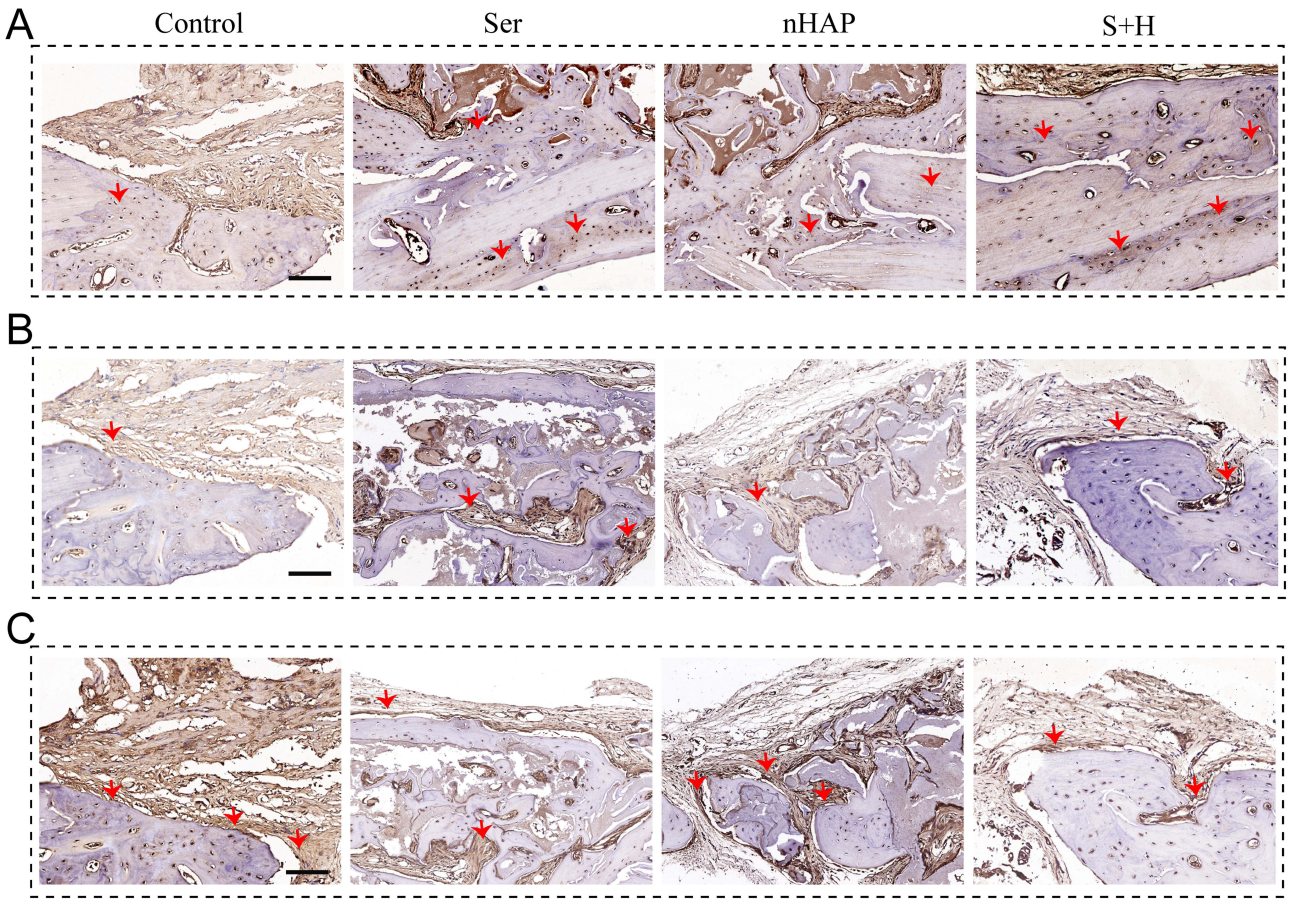

Figure 7 Immunohistochemical staining of COLI, Arg-1, and iNOS after implantation for 8 weeks. (**A–C**) Representative photographs of immunohistochemical staining of (**A**) COLI, (**B**) Arg-1, and (**C**) iNOS. Scale bar = 100μm. Red arrows represent relatively typical protein staining areas.

scaffolds were approximately 66.68% and 61.98%, respectively. These particles filled the empty area, resulting in a decrease in pore size and porosity (Table S2), resembling the porosity value of human bone, which contains 45% to 65% pores and permits easy passage of oxygen, nutrients, and wastes.[32–34]

The Alg hydrogel had absorbance peaks at 2929 and 1612 cm^{-1}, which represent N-H and COONa vibrations and are traditional absorbance peaks of alginate.[35] The absorbance bands at 1612 and 1418 cm^{-1} observed in the FTIR spectrum of the Alg/GO hydrogel represent the vibration of the N-H of alginate,[36] but the characteristic absorbance bands of GO were not observed, mainly as a consequence of the lower amount of GO in the hydrogel than in the natural polymer alginate (Figure 1C and D). Studies have indicated that the characteristic absorption peaks of sericin are at 1656, 1535, and 1239 cm^{-1}, representing the characteristic amide I, II, and III peaks, respectively.[37] As shown in Figure 1D, the absorption peak of sericin in the corresponding hydrogels was marginally altered from 1656 to 1611 cm^{-1} and the number of random coil absorption peaks decreased. Research showed that there are various functional groups in sericin, including carboxyl, hydroxyl, and amino groups, that can form electronic interactions and hydrogen bonds with the chemical bonds belonging to GO (eg, carboxyl, epoxy, and hydroxyl groups), so sericin may interact with GO to cause the alter of the absorption peak of sericin (1656 to 1611 cm^{-1}).[28] Interestingly, the characteristic absorbance band of 1611 cm^{-1} represents the stable β-sheet structure presented in the amide I region of sericin,[37] therefore, this alter caused by the interaction between sericin and GO also made the structure of the nanocomposite hydrogel more stable Additionally, the bands at 1034 cm^{-1} existed in the corresponding hydrogel was associated with the P=O of nHAP (Figure 1D).[38]

The results of strain–stress curves illustrated that the combination with nHAP could dramatically increase the mechanical property of scaffolds (Figure 1E), which may contribute to promoting bone growth.[39] In addition, the storage

moduli of all the prepared hydrogels were greater than those of the corresponding loss moduli (Figure 1F), confirming the formation of hydrogels.[40] Hydrogels containing sericin are likely to be less stiff due to the destruction of the electrostatic connections between two polymeric materials generated by the protein, while nHAP is promising for providing better elasticity and a more stable network structure.[41]

One crucial factor for assessing the applications of biomaterials is hydrophilicity, which is vital for the absorption of bodily fluids and the transfer of cell nutrients and metabolites.[42] The swelling activity of the hydrogel scaffolds is affected by a variety of factors, such as pore width, porosity, and the hydrophilicity properties of the material.[43,44] In this study, a decrease in swelling capability was observed in the composite gel scaffold due to their lower porosity compared with the Alg gel (Figure 1G). Additionally, the hydrophobicity of nHAP particles in the corresponding scaffold could somewhat weaken the ability of the hydrogel to absorb water.[45] Based on previous research, sericin is a hydrophilic protein polymer, which is a glycoprotein including essential amino acids and a high content of hydrophilic amino acids, especially serine, which makes it water-soluble.[16,18] According to the results of our study, although the porosity of Alg/GO/Ser/nHAP (61.98%) was lower than that of Alg/GO/nHAP (66.68%), its swelling rate was unexpectedly higher than that of Alg/GO/nHAP. We speculate that, compared to Alg/GO/nHAP, it was the highly hydrophilic property of the sericin in Alg/GO/Ser/nHAP that allowed it to adsorb more liquid, and the final swelling rate of Alg/GO/Ser/nHAP was slightly higher than that of Alg/GO/nHAP, which improve the performance of the scaffold applied to bone tissue engineering. In addition, the performance of bone tissue regeneration could be influenced by the degradation speed of the scaffolds. The lysozymes included in physiological fluids and tissues lead the porous scaffold to breakdown, so hydrogels can disintegrate naturally when the tissue regenerates.[46] The result revealed that the degradation of the Alg/GO/Ser/nHAP gel reached approximately 45% within 56 days (Figure 1H). However, Alg hydrogel, as a result of its single structure and weak stability, was quickly degraded with a maximum degradation rate of approximately 90% (Figure 1H). Consequently, its tissue engineering application is too limited because it does not support the local microenvironment well. Therefore, the Alg/GO/Ser/nHAP composite gel scaffold is promising for bone regeneration due to its complicated structure, high stability, and delayed degradation properties.

For tissue regeneration in vivo, the proliferation and adhesion of cells are also essential,[47] so we examined the bioactivity and spreading of BMSCs cultured with different hydrogels. According to the results, all hydrogel scaffolds promoted the proliferation and extension of BMSCs (Figure 2A–C). Previous studies showed that surface properties, such as chemistry, roughness, texture, and porosity, mostly impact the proliferation, viability, and differentiation of cells.[48] Considering these factors, protein-based nanocarriers, such as nHAP have been extensively researched for nanoformulation manufacturing because of their intrinsic features, such as low toxicity and biocompatibility.[49] Moreover, silk sericin is frequently used in tissue engineering due to its mitogenic action, which promotes the proliferation of cells.[20] Additionally, GO increases the attachment and proliferation of cells, making it a powerful growth booster.[50] These findings imply that the nanocomposite scaffold developed in this study could be biocompatible with cells. Furthermore, diverse oxygen-containing functional groups, such as hydroxyl, carboxylic, and carbonyl groups, which serve as adhesion sites for biological molecules and cells, are included in the complex framework of GO.[51] In addition, the amphiphilic property of GO, along with its large surface area, not only makes it an adaptable, biocompatible intracellular carrier but also empowers the expansion of cells, demonstrating that GO has the potential to support the spreading of cells.[52] In summary, our results showed that all nanocomposite hydrogels had good performance in terms of proliferation, adhesion, and biocompatibility, which could foster a microenvironment that is conducive to the expansion and proliferation of cells.

Biomaterials are becoming increasingly important in regenerative techniques; nevertheless, the implantation of biomaterials and devices inevitably fails due to the foreign body reaction (FBR) induced by the host,[53] so a substantial amount of research has been conducted on the regulation of the immunological responses of implanted materials. The modulation of macrophage responses is of particular importance because it is related to not only the FBR but also tissue repair.[6] In terms of bone implants, excessive M1 macrophages have been reported to induce the absorption of bone tissue, which is a major contributor to implant loosening and implantation failure.[54] In contrast, M2 macrophage polarization has been confirmed to construct an anti-inflammatory microenvironment to promote bone regeneration.[55] Sericin has been observed to have a mild inflammatory and low immunological response as a result of its high serine

content.[17] Accordingly, the application of sericin may have a positive impact on osteoimmunomodulation, which is promising for better implant integration between implants and tissues.[56] Our results confirmed that the hydrogel including sericin (eg, Ser and S+H groups) efficiently induced macrophage differentiation from the M1-type to the M2-type to inhibit inflammation (Figure 3A–F). Based on previous research, silk sericin of Bombyx mori has been evaluated as a promising biomaterial with ideal biocompatibility and weak immunogenicity.[57] Composite scaffolds containing sericin were shown to decrease the expression of specific proinflammatory markers and stimulate the expression of the anti-inflammatory marker IL-10 on LPS-stimulated macrophages.[56] Sericin has been found to prevent proinflammatory cytokine release by negatively regulating the NF-κB and MAPK pathways, promoting macrophage M2 polarization and migration.[28] Interestingly, there is evidence that molecules in the NF-κB pathway regulate inflammation and macrophage polarization, particularly the receptor activator of NF-κB ligand, which is crucial in immunological diseases that influence bone repair and is characterized as a key element that connects the bone and immune systems.[58] These discoveries demonstrate that these scaffolds including sericin (eg, the Ser and S+H group) may stimulate macrophage polarization from the M1 to the M2 phenotype to establish an anti-inflammatory microenvironment for bone tissue regeneration.

Studies showed that nHAP can directly induce osteogenic differentiation of BMSCs.[22] Our results revealed that both the nHAP and Ser group could promote BMSCs to differentiate into osteoblasts, while the direct osteogenesis induction effect of the nHAP group seemed to be better than that of the Ser group (Figure 4A–I). Hydroxyapatite is the most predominant inorganic component of bone, with outstanding biocompatibility, osteoinduction, and mechanical strength, and it has been widely employed in orthopedic and dental materials.[21,59] Studies revealed that the Notch signaling pathway[60] and the Erk1/2 signaling pathway[61] were related to the mechanism of nHAP osteogenesis induction. However, the osteogenic differentiation-inducing ability of sericin is limited.[16] Therefore, nHAP directly and significantly enhances the osteogenic differentiation of BMSCs. In addition, GO has a porous, folded surface and high hardness, allowing it to induce mechanical stimulation, resulting in a chain of responses that induce osteogenic differentiation.[25] Furthermore, extracellular matrix modification[62] and regulation of signalling pathways, such as PI3K/Akt/GSK-3/catenin,[63] Wnt/β-catenin,[64] and BMP,[65] may all play a role in the underlying mechanisms of the regulation of osteogenesis induced by GO. These investigations indicate that the osteoinduction activity of GO can be achieved by a multitude of separate pathways. Overall, the nanocomposite hydrogels developed in this study exhibited direct and synergistic osteogenesis effects.

Research has confirmed that macrophages occupy a key regulatory position during all processes of bone formation and can stimulate bone regeneration by releasing various cytokines.[2,66] Our results indicated that the osteogenesis induction produced by cocultivation of BMSCs with the MCM of the Ser group was better than that with the MCM of the nHAP group (Figure 5A–J). Our previous studies revealed that sericin promoted macrophage M2 polarization (Figure 3A–F), while nHAP exerted direct osteoinduction properties (Figure 4A–I). The findings of cocultivation with macrophages in this study demonstrate that the hydrogel with osteoimmunomodulatory capabilities (eg, the Ser group) performed better than the hydrogel with direct osteogenesis induction characteristics (eg, the nHAP group) in terms of promotion of bone regeneration, which corresponds to observations from prior research.[13,28] Macrophages can deliver osteogenesis molecules, such as BMP-2,[9] TGF-β,[67] and VEGF,[68] after induction of the M2 phenotype to directly promote osteogenic differentiation of BMSCs. Additionally, many anti-inflammatory cytokines, including IL-4,[69] IL-10,[9] and IL-13,[70] generated by M2 macrophages were found to prevent excessive inflammation and help induce osteogenesis. These studies show that macrophages can not only directly induce the osteogenic differentiation of BMSCs but also accelerate bone regeneration by suppressing the immune response. The previous results in this study showed that sericin could regulate the transition of macrophages from the M1 to the M2 phenotype to prevent a negative host immune reaction. In this case, we speculate that sericin, as an anti-inflammatory chemical that can regulate the differentiation of M2 macrophages to form a beneficial osteoimmunomodulatory environment, can stimulate osteogenesis in multiple ways, not only in a direct manner as is the case for nHAP, which explains why the effect of the Ser group on osteogenesis was better than that of the HAP group when cocultured with macrophages. In addition, these findings of osteogenic differentiation-related experiments revealed that the S+H group exhibited the strongest osteogenesis induction ability (Figure 5B–J), further indicating that the appropriate osteoimmunomodulatory microenvironment established by sericin coupled with the osteoinductive atmosphere induced by nHAP could contribute to immunoenhanced osteogenesis.

Therefore, these results imply that the synergistic interactions between direct osteogenesis activity and immune-induced osteogenesis effects may be more beneficial for bone repair than focusing on a single mechanism.[11,13]

In tissue regeneration, chronic inflammation originating from inappropriate implants contributes to the emergence of fibrous encapsulation surrounding the implant, triggering osseointegration failure.[6,8] Our results in vivo demonstrated that more fresh bone tissue and Arg-1 protein, less fibrous layer and iNOS protein were observed in the Ser group compared to the nHAP group (Figures 6A–D and 7A–C), revealing that the Ser group not only inhibited the local inflammatory response induced by the implant but also promoted bone tissue regeneration through immunomodulatory osteogenesis effect, which may have a greater advantage than the direct osteogenesis impact of the nHAP group for bone tissue regeneration. Recent studies suggest that the accurate and continuous stimulation of the differentiation of macrophages from the M1 phenotype to the M2 phenotype can hasten the process of bone healing in comparison to the simple osteoinductive effect of the implant.[71,72] Then, it was reported that the M2 macrophage phenotype not only releases various anti-inflammatory molecules, including Arg-1,[11] IL-4,[69] and IL-10,[9] to prevent local inflammation assisting in osteogenesis induction but also secretes osteogenesis factors, such as BMP-2,[9] TGF-β,[67] and VEGF,[68] directly stimulating the osteogenic differentiation of recruited BMSCs. The recruited BMSCs could also influence the local immune microenvironment by producing factors, such as BMP-2 and IL-4, which in turn activated the differentiation of macrophages to the anti-inflammatory M2 phenotype, leading to a positive feedback mechanism to further promote bone regeneration.[73,74] Therefore, we speculate that in addition to direct osteogenesis induction and promoting bone regrowth through anti-inflammatory activity, there is also a positive feedback loop between macrophages and BMSCs to stimulate osteogenesis. Importantly, we confirmed that sericin could induce the transition of macrophages from the M1 to the M2 phenotype, which further reveals why the Ser group had a stronger impact on osteogenesis than the nHAP group in vivo. Thus, these discoveries highlight the significance of the ability of implanted biomaterials to modulate the immune microenvironment during bone defect repair. In addition, the results in vivo also showed that the S +H hydrogel combination of sericin and nHAP was the most effective in promoting bone regeneration based on all of the in vivo experimental results (Figures 6A–D and 7A), presumably as a result of the synergistic effect between osteoinductive nHAP and immunoactive sericin, while a mono-element (eg, the Ser or nHAP group) may not establish the most supportive immunomodulatory microenvironment for the formation of new bone, which assumes that the cooperation effects of direct osteoinduction in conjunction with immune-induced osteogenesis are critical to bone regeneration in vivo.

We are the first to prepare bone defect implants by combining sodium alginate and graphene oxide as base hydrogel scaffolds, which were further modified with silk sericin which can regulate the transformation of macrophage phenotype and nHAP which can induce osteogenesis directly of BMSCs. In prior studies, silk sericin was only partially developed as a single hydrogel scaffold[75] or as an effector protein to facilitate BMSCs migration,[76] without fully exploiting the anti-inflammatory properties of silk sericin. Furthermore, other studies relied on the exogenous introductions of cells with immune-modulatory functions[77] or molecules with inflammation-suppressing properties into the hydrogel scaffold without considering the anti-inflammatory properties of the hydrogel constituents themselves.[78] In contrast to previous studies, we not only took full advantage of the osteogenic induction of nHAP but also took into account the inflammatory response induced by the exogenous implanted scaffold, rather than merely concentrating on the osteogenic induction by the implant. In addition to utilizing the basic gel-forming properties of these natural polymers, our study fully exploited the important property of the material components that comprised hydrogel scaffold, that is the regulatory effect on the phenotypic transformation of macrophages, thus avoiding the exogenous introduction of anti-inflammatory related molecules which may be poorly stable and easily degraded or the preparation of complex and expensive cellular exosomes. In conclusion, our study provides a new paradigm for composite hydrogel materials to achieve macrophage modulation to improve the immune microenvironment of bone defects for effective bone regeneration in tissue engineering.

Overall, in vivo and in vitro experiments demonstrated that the Alg/GO/Ser/nHAP nanocomposite hydrogel inhibited the inflammatory response around implants and accelerated bone defect repair by promoting the transformation of M1 macrophages into M2 macrophages. Although much more research is still necessary to evaluate the underlying

mechanisms of osteoimmunomodulation, the results of our study provide a fresh perspective on how to develop implants for bone tissue regeneration that are both immunoreactive and osteoinductive.

Conclusion

In our study, using the cross-linking system of EDTA-2Ca/GDL, we developed nanocomposite hydrogels (Alg/GO/Ser/nHAP) with both immunomodulatory and osteoinductive properties. The results of both the in vivo and in vitro investigations confirmed that the fabricated hydrogel showed ideal biocompatibility, and the sericin in the nanocomposite hydrogels created a positive osteoimmune microenvironment by switching the phenotype of macrophages from M1 to M2, which improved the process of osseointegration between the bone and implant interface, thus initiating and inducing BMSCs differentiation to osteoblasts. More importantly, the combination of nHAP and sericin in the nanocomposite hydrogel further stimulated osteogenesis and bone regrowth, illustrating that the synergistic relationship between the direct osteogenesis activity of nHAP and the immune-induced osteogenesis effect of sericin was extremely significant for bone defect healing. Overall, a desirable osteoimmunomodulatory atmosphere for bone regeneration was established by the nanocomposite hydrogel (Alg/GO/Ser/nHAP) through its ability to regulate the phenotypic conversion of macrophages, which provides a new concept for the design of immunomodulatory properties and osteogenesis capabilities in bone tissue engineering implants.

Abbreviations

Alg, Alginate; ALP, Alkaline phosphatase; Arg-1, Arginine-1; ARS, Alizarin red staining; BMP-2, Bone morphogenetic protein-2; BMP-4, Bone morphogenetic protein-4; BMSCs, Bone marrow stem cells; BTE, Bone tissue engineering; COL I, Collagen type I; EDTA, Ethylene diamine tetraacetic acid; FBR, Foreign body reaction; GO, Graphene oxide; H&E, Hematoxylin–eosin; IF, Immunofluorescence; IFN-γ, Interferon-gamma; IHC, Immunohistochemistry. IL-1, Interleukin 1; IL-4, Interleukin 4; IL-6, Interleukin 6; IL-10, Interleukin 10; iNOS, inducible nitric oxide synthase; LPS, Lipopolysaccharide; MAPK, Mitogen-activated protein kinase; Micro-CT, Micro-computed tomography; nHAP, nano hydroxyapatite; OCN, Osteocalcin; qRT-PCR, Quantitative real-time polymerase chain reaction; RunX2, Runt-related transcription factor 2; Ser, Sericin; TGF-β, Transforming growth factor-β; TNF-α, Tumor necrosis factor-alpha; VEGF, Vascular endothelial growth factor.

Acknowledgments

This work was financially supported by the National Natural Science Foundation of China (Grant/Award Number:81971169) and the Shanghai Science and Technology Commission (Grant/Award Number: 20Y11901800). The authors sincerely appreciate the assistance of experts from the School of Basic Medicine, Tongji University, and the Public Instrument Platform of Advanced Research Institute of Translational Medicine, Tongji University.

Disclosure

The authors report no conflicts of interest in this work.

References

1. Zhao C, Liu W, Zhu M, Wu C, Zhu Y. Bioceramic-based scaffolds with antibacterial function for bone tissue engineering: a review. *Bioact Mater*. 2022;18:383–398.
2. Niu Y, Wang Z, Shi Y, Dong L, Wang C. Modulating macrophage activities to promote endogenous bone regeneration: biological mechanisms and engineering approaches. *Bioact Mater*. 2021;6:244–261. doi:10.1016/j.bioactmat.2020.08.012
3. Bose S, Sarkar N. Natural medicinal compounds in bone tissue engineering. *Trends Biotechnol*. 2020;38:404–417. doi:10.1016/j.tibtech.2019.11.005
4. Zhang L, Yang G, Johnson BN, Jia X. Three-dimensional (3D) printed scaffold and material selection for bone repair. *Acta Biomater*. 2019;84:16–33. doi:10.1016/j.actbio.2018.11.039
5. Hao Z, Li H, Wang Y, et al. Supramolecular peptide nanofiber hydrogels for bone tissue engineering: from multihierarchical fabrications to comprehensive applications. *Adv Sci*. 2022;9:e2103820. doi:10.1002/advs.202103820
6. Martin KE, García AJ. Macrophage phenotypes in tissue repair and the foreign body response: implications for biomaterial-based regenerative medicine strategies. *Acta Biomater*. 2021;133:4–16. doi:10.1016/j.actbio.2021.03.038
7. Mestres G, Carter SD, Hailer NP, Diez-Escudero A. A practical guide for evaluating the osteoimmunomodulatory properties of biomaterials. *Acta Biomater*. 2021;130:115–137. doi:10.1016/j.actbio.2021.05.038

8. Xie Y, Hu C, Feng Y, et al. Osteoimmunomodulatory effects of biomaterial modification strategies on macrophage polarization and bone regeneration. *Regener Biomater*. 2020;7:233–245. doi:10.1093/rb/rbaa006
9. Zhu Y, Liang H, Liu X, et al. Regulation of macrophage polarization through surface topography design to facilitate implant-to-bone osteointegration. *Sci Adv*. 2021;7:eabf6654. doi:10.1126/sciadv.abf6654
10. Sadowska JM, Ginebra MP. Inflammation and biomaterials: role of the immune response in bone regeneration by inorganic scaffolds. *J Mater Chem B*. 2020;8:9404–9427. doi:10.1039/D0TB01379J
11. Fan L, Guan P, Xiao C, et al. Exosome-functionalized polyetheretherketone-based implant with immunomodulatory property for enhancing osseointegration. *Bioact Mater*. 2021;6:2754–2766. doi:10.1016/j.bioactmat.2021.02.005
12. Patel DK, Dutta SD, Hexiu J, Ganguly K, Lim KT. 3D-printable chitosan/silk fibroin/cellulose nanoparticle scaffolds for bone regeneration via M2 macrophage polarization. *Carbohydr Polym*. 2022;281:119077. doi:10.1016/j.carbpol.2021.119077
13. Wang T, Bai J, Lu M, et al. Engineering immunomodulatory and osteoinductive implant surfaces via mussel adhesion-mediated ion coordination and molecular clicking. *Nat Commun*. 2022;13:160. doi:10.1038/s41467-021-27816-1
14. Wu Z, Bai J, Ge G, et al. Regulating macrophage polarization in high glucose microenvironment using lithium-modified bioglass-hydrogel for diabetic bone regeneration. *Adv Healthcare Mater*. 2022;11:e2200298. doi:10.1002/adhm.202200298
15. He J, Chen G, Liu M, et al. Scaffold strategies for modulating immune microenvironment during bone regeneration. *Mater Sci Eng C*. 2020;108:110411. doi:10.1016/j.msec.2019.110411
16. Chouhan D, Mandal BB. Silk biomaterials in wound healing and skin regeneration therapeutics: from bench to bedside. *Acta Biomater*. 2020;103:24–51. doi:10.1016/j.actbio.2019.11.050
17. Zhang D, Chen Q, Zhang W, et al. Silk-inspired β-peptide materials resist fouling and the foreign-body response. *Angew Chem Int Ed Engl*. 2020;59:9586–9593. doi:10.1002/anie.202000416
18. Lamboni L, Gauthier M, Yang G, Wang Q. Silk sericin: a versatile material for tissue engineering and drug delivery. *Biotechnol Adv*. 2015;33:1855–1867. doi:10.1016/j.biotechadv.2015.10.014
19. Zhang D, Chen Q, Bi Y, et al. Bio-inspired poly-DL-serine materials resist the foreign-body response. *Nat Commun*. 2021;12:5327. doi:10.1038/s41467-021-25581-9
20. Das G, Shin HS, Campos EV, et al. Sericin based nanoformulations: a comprehensive review on molecular mechanisms of interaction with organisms to biological applications. *J Nanobiotechnol*. 2021;19:30. doi:10.1186/s12951-021-00774-y
21. Farokhi M, Mottaghitalab F, Samani S, et al. Silk fibroin/hydroxyapatite composites for bone tissue engineering. *Biotechnol Adv*. 2018;36:68–91. doi:10.1016/j.biotechadv.2017.10.001
22. Cho YS, Quan ML, Kang NU, et al. Strategy for enhancing mechanical properties and bone regeneration of 3D polycaprolactone kagome scaffold: nano hydroxyapatite composite and its exposure. *Eur Polym J*. 2020;134:12. doi:10.1016/j.eurpolymj.2020.109814
23. Hernández-González AC, Téllez-Jurado L, Rodríguez-Lorenzo LM. Alginate hydrogels for bone tissue engineering, from injectables to bioprinting: a review. *Carbohydr Polym*. 2020;229:115514. doi:10.1016/j.carbpol.2019.115514
24. Bressan E, Ferroni L, Gardin C, et al. Graphene based scaffolds effects on stem cells commitment. *J Transl Med*. 2014;12:296. doi:10.1186/s12967-014-0296-9
25. Lee WC, Lim CH, Shi H, et al. Origin of enhanced stem cell growth and differentiation on graphene and graphene oxide. *ACS nano*. 2011;5:7334–7341. doi:10.1021/nn202190c
26. Liu W, Li J, Cheng M, et al. A surface-engineered polyetheretherketone biomaterial implant with direct and immunoregulatory antibacterial activity against methicillin-resistant Staphylococcus aureus. *Biomaterials*. 2019;208:8–20. doi:10.1016/j.biomaterials.2019.04.008
27. Anderson JM, Rodriguez A, Chang DT. Foreign body reaction to biomaterials. *Semin Immunol*. 2008;20:86–100. doi:10.1016/j.smim.2007.11.004
28. Jiang LB, Ding SL, Ding W, et al. Injectable sericin based nanocomposite hydrogel for multi-modal imaging-guided immunomodulatory bone regeneration. *Chem Eng J*. 2021;418:19.
29. Cao L, Lu W, Mata A, Nishinari K, Fang Y. Egg-box model-based gelation of alginate and pectin: a review. *Carbohydr Polym*. 2020;242:116389. doi:10.1016/j.carbpol.2020.116389
30. Lee KY, Mooney DJ. Alginate: properties and biomedical applications. *Prog Polym Sci*. 2012;37:106–126. doi:10.1016/j.progpolymsci.2011.06.003
31. Li Z, Du T, Ruan C, Niu X. Bioinspired mineralized collagen scaffolds for bone tissue engineering. *Bioact Mater*. 2021;6:1491–1511. doi:10.1016/j.bioactmat.2020.11.004
32. Palacio-Mancheno PE, Larriera AI, Doty SB, et al. 3D assessment of cortical bone porosity and tissue mineral density using high-resolution μCT: effects of resolution and threshold method. *J Bone Miner Res*. 2014;29:142–150. doi:10.1002/jbmr.2012
33. Collins MN, Ren G, Young K, et al. Scaffold fabrication technologies and structure/function properties in bone tissue engineering. *Adv Funct Mater*. 2021;31:2010609.
34. Wang C, Huang W, Zhou Y, et al. 3D printing of bone tissue engineering scaffolds. *Bioact Mater*. 2020;5:82–91. doi:10.1016/j.bioactmat.2020.01.004
35. KhorramiN K, Radi M, Amiri S, McClements DJ. Fabrication and characterization of alginate-based films functionalized with nanostructured lipid carriers. *Int J Biol Macromol*. 2021;182:373–384. doi:10.1016/j.ijbiomac.2021.03.159
36. Lawrie G, Keen I, Drew B, et al. Interactions between alginate and chitosan biopolymers characterized using FTIR and XPS. *Biomacromolecules*. 2007;8:2533–2541. doi:10.1021/bm070014y
37. Wang X, Tang J, Huang J, Hui M. Production and characterization of bacterial cellulose membranes with hyaluronic acid and silk sericin. *Colloids Surf B*. 2020;195:111273. doi:10.1016/j.colsurfb.2020.111273
38. Alicka M, Sobierajska P, Kornicka K, Wiglusz RJ, Marycz K. Lithium ions (Li (+)) and nanohydroxyapatite (nHAp) doped with Li (+) enhance expression of late osteogenic markers in adipose-derived stem cells. Potential theranostic application of nHAp doped with Li (+) and co-doped with europium (III) and samarium (III) ions. *Mater Sci Eng C*. 2019;99:1257–1273.
39. Santana-Melo GF, Rodrigues BVM, da Silva E, et al. Electrospun ultrathin PBAT/nHAp fibers influenced the in vitro and in vivo osteogenesis and improved the mechanical properties of neoformed bone. *Colloids Surf B*. 2017;155:544–552. doi:10.1016/j.colsurfb.2017.04.053
40. Zhang Y, Zhang H, Zou Q, Xing R, Jiao T, Yan X. An injectable dipeptide-fullerene supramolecular hydrogel for photodynamic antibacterial therapy. *J Mater Chem B*. 2018;6:7335–7342. doi:10.1039/C8TB01487F

41. Shahbazarab Z, Teimouri A, Chermahini AN, Azadi M. Fabrication and characterization of nanobiocomposite scaffold of zein/chitosan/nanohydroxyapatite prepared by freeze-drying method for bone tissue engineering. *Int J Biol Macromol*. 2018;108:1017–1027. doi:10.1016/j.ijbiomac.2017.11.017
42. Ji C, Khademhosseini A, Dehghani F. Enhancing cell penetration and proliferation in chitosan hydrogels for tissue engineering applications. *Biomaterials*. 2011;32:9719–9729. doi:10.1016/j.biomaterials.2011.09.003
43. Felfel RM, Gideon-Adeniyi MJ, Zakir Hossain K, Roberts GAF, Grant DM. Structural, mechanical and swelling characteristics of 3D scaffolds from chitosan-agarose blends. *Carbohydr Polym*. 2019;204:59–67. doi:10.1016/j.carbpol.2018.10.002
44. Patel S, Srivastava S, Singh MR, Singh D. Preparation and optimization of chitosan-gelatin films for sustained delivery of lupeol for wound healing. *Int J Biol Macromol*. 2018;107:1888–1897.
45. Mahato A, Sandy Z, Bysakh S, et al. Development of nano-porous hydroxyapatite coated e-glass for potential bone-tissue engineering application: an in vitro approach. *Mater Sci Eng C*. 2020;111:110764. doi:10.1016/j.msec.2020.110764
46. Yang D, Xiao J, Wang B, Li L, Kong X, Liao J. The immune reaction and degradation fate of scaffold in cartilage/bone tissue engineering. *Mater Sci Eng C*. 2019;104:109927.
47. Zhu G, Zhang T, Chen M, et al. Bone physiological microenvironment and healing mechanism: basis for future bone-tissue engineering scaffolds. *Bioact Mater*. 2021;6:4110–4140. doi:10.1016/j.bioactmat.2021.03.043
48. Selvaraj S, Fathima NN. Fenugreek incorporated silk fibroin Nanofibers-A potential antioxidant scaffold for enhanced wound healing. *ACS Appl Mater Interfaces*. 2017;9:5916–5926. doi:10.1021/acsami.6b16306
49. Sathiyavimal S, Vasantharaj S, LewisOscar F, Pugazhendhi A, Subashkumar R. Biosynthesis and characterization of hydroxyapatite and its composite (hydroxyapatite-gelatin-chitosan-fibrin-bone ash) for bone tissue engineering applications. *Int J Biol Macromol*. 2019;129:844–852. doi:10.1016/j.ijbiomac.2019.02.058
50. Ruiz ON, Fernando KA, Wang B, et al. Graphene oxide: a nonspecific enhancer of cellular growth. *ACS nano*. 2011;5:8100–8107. doi:10.1021/nn202699t
51. Singh DP, Herrera CE, Singh B, Singh S, Singh RK, Kumar R. Graphene oxide: an efficient material and recent approach for biotechnological and biomedical applications. *Mater Sci Eng C*. 2018;86:173–197.
52. Reina G, González-Domínguez JM, Criado A, Vázquez E, Bianco A, Prato M. Promises, facts and challenges for graphene in biomedical applications. *Chem Soc Rev*. 2017;46:4400–4416. doi:10.1039/C7CS00363C
53. Balabiyev A, Podolnikova NP, Kilbourne JA, et al. Fibrin polymer on the surface of biomaterial implants drives the foreign body reaction. *Biomaterials*. 2021;277:121087.
54. Ding C, Yang C, Cheng T, et al. Macrophage-biomimetic porous Se@SiO(2) nanocomposites for dual modal immunotherapy against inflammatory osteolysis. *J Nanobiotechnol*. 2021;19:382. doi:10.1186/s12951-021-01128-4
55. Antonios JK, Yao Z, Li C, Rao AJ, Goodman SB. Macrophage polarization in response to wear particles in vitro. *Cell Mol Immunol*. 2013;10:471–482. doi:10.1038/cmi.2013.39
56. Chachlioutaki K, Karavasili C, Adamoudi E, et al. Silk sericin/PLGA electrospun scaffolds with anti-inflammatory drug-eluting properties for periodontal tissue engineering. *Mater Sci Eng C*. 2022;133:112723.
57. Huang W, Ling S, Li C, Omenetto FG, Kaplan DL. Silkworm silk-based materials and devices generated using bio-nanotechnology. *Chem Soc Rev*. 2018;47:6486–6504. doi:10.1039/C8CS00187A
58. Okamoto K, Nakashima T, Shinohara M, et al. Osteoimmunology: the conceptual framework unifying the immune and skeletal systems. *Physiol Rev*. 2017;97:1295–1349.
59. Kim H, Hwangbo H, Koo Y, Kim G. Fabrication of mechanically reinforced gelatin/hydroxyapatite bio-composite scaffolds by core/shell nozzle printing for bone tissue engineering. *Int J Mol Sci*. 2020;21:3401. doi:10.3390/ijms21093401
60. Zou Z, Wang L, Zhou Z, et al. Simultaneous incorporation of PTH (1-34) and nano-hydroxyapatite into Chitosan/Alginate Hydrogels for efficient bone regeneration. *Bioact Mater*. 2021;6:1839–1851. doi:10.1016/j.bioactmat.2020.11.021
61. Boller LA, Shiels SM, Florian DC, et al. Effects of nanocrystalline hydroxyapatite concentration and skeletal site on bone and cartilage formation in rats. *Acta Biomater*. 2021;130:485–496. doi:10.1016/j.actbio.2021.05.056
62. Newby SD, Masi T, Griffin CD, et al. Functionalized graphene nanoparticles induce human mesenchymal stem cells to express distinct extracellular matrix proteins mediating osteogenesis. *Int J Nanomed*. 2020;15:2501–2513. doi:10.2147/IJN.S245801
63. Wu X, Zheng S, Ye Y, Wu Y, Lin K, Su J. Enhanced osteogenic differentiation and bone regeneration of poly (lactic-co-glycolic acid) by graphene via activation of PI3K/Akt/GSK-3β/β-catenin signal circuit. *Biomater Sci*. 2018;6:1147–1158. doi:10.1039/C8BM00127H
64. Bordoni V, Reina G, Orecchioni M, et al. Stimulation of bone formation by monocyte-activator functionalized graphene oxide in vivo. *Nanoscale*. 2019;11:19408–19421. doi:10.1039/C9NR03975A
65. Wu J, Zheng A, Liu Y, et al. Enhanced bone regeneration of the silk fibroin electrospun scaffolds through the modification of the graphene oxide functionalized by BMP-2 peptide. *Int J Nanomed*. 2019;14:733–751. doi:10.2147/IJN.S187664
66. Pajarinen J, Lin T, Gibon E, et al. Mesenchymal stem cell-macrophage crosstalk and bone healing. *Biomaterials*. 2019;196:80–89. doi:10.1016/j.biomaterials.2017.12.025
67. Chen M, Zhang Y, Zhou P, et al. Substrate stiffness modulates bone marrow-derived macrophage polarization through NF-κB signaling pathway. *Bioact Mater*. 2020;5:880–890. doi:10.1016/j.bioactmat.2020.05.004
68. Hao S, Meng J, Zhang Y, et al. Macrophage phenotypic mechanomodulation of enhancing bone regeneration by superparamagnetic scaffold upon magnetization. *Biomaterials*. 2017;140:16–25. doi:10.1016/j.biomaterials.2017.06.013
69. Jin SS, He DQ, Luo D, et al. A biomimetic hierarchical nanointerface orchestrates macrophage polarization and mesenchymal stem cell recruitment to promote endogenous bone regeneration. *ACS nano*. 2019;13:6581–6595. doi:10.1021/acsnano.9b00489
70. Kazimierczak P, Koziol M, Przekora A. The chitosan/Agarose/NanoHA bone scaffold-induced M2 macrophage polarization and its effect on osteogenic differentiation in vitro. *Int J Mol Sci*. 2021;22:1109. doi:10.3390/ijms22031109
71. Zheng ZW, Chen YH, Wu DY, et al. Development of an accurate and proactive immunomodulatory strategy to improve bone substitute material-mediated osteogenesis and angiogenesis. *Theranostics*. 2018;8:5482–5500. doi:10.7150/thno.28315
72. Spiller KL, Nassiri S, Witherel CE, et al. Sequential delivery of immunomodulatory cytokines to facilitate the M1-to-M2 transition of macrophages and enhance vascularization of bone scaffolds. *Biomaterials*. 2015;37:194–207. doi:10.1016/j.biomaterials.2014.10.017

73. Zou M, Sun J, Xiang Z. Induction of M2-type macrophage differentiation for bone defect repair via an interpenetration network hydrogel with a GO-based controlled release system. *Adv Healthcare Mater*. 2021;10:e2001502. doi:10.1002/adhm.202001502
74. Chen R, Hao Z, Wang Y, et al. Mesenchymal stem cell-immune cell interaction and related modulations for bone tissue engineering. *Stem Cells Int*. 2022;2022:7153584. doi:10.1155/2022/7153584
75. Zhang HJ, Li FS, Wang F, et al. Transgenic PDGF-BB sericin hydrogel potentiates bone regeneration of BMP9-stimulated mesenchymal stem cells through a crosstalk of the Smad-STAT pathways. *Regener Biomater*. 2023;10:rbac095. doi:10.1093/rb/rbac095
76. Qi C, Deng Y, Xu L, et al. A sericin/ graphene oxide composite scaffold as a biomimetic extracellular matrix for structural and functional repair of calvarial bone. *Theranostics*. 2020;10:741–756. doi:10.7150/thno.39502
77. Sun J, Li L, Xing F, et al. Graphene oxide-modified silk fibroin/nanohydroxyapatite scaffold loaded with urine-derived stem cells for immunomodulation and bone regeneration. *Stem Cell Res Ther*. 2021;12:591. doi:10.1186/s13287-021-02634-w
78. Liu Y, Zhang Y, Zheng Z, et al. Incorporation of NGR1 promotes bone regeneration of injectable HA/nHAp hydrogels by anti-inflammation regulation via a MAPK/ERK signaling pathway. *Front Bioeng Biotechnol*. 2022;10:992961. doi:10.3389/fbioe.2022.992961